


Microstructural and mechanical analysis of GMAW short-circuit welding on dual phase DP1000 steels for automotive applications

 <https://doi.org/10.56238/sevned2024.010-048>

Elizângela de Macêdo Brito¹, Ângela Maria de Arruda², Ayrton de Sá Brandim³, Daiany Jacinta de Carvalho⁴, Luiz Gustavo Mafra de Ávila⁵, Louriel Oliveira Vilarinho⁶, Diandro Bailoni Fernandes⁷, Edimundo Beneletti Filho⁸, Daniel Dominices Baia Gomes de Souza⁹, Joyce Antunes da Silva¹⁰, Henrique Nardon Ferraresi¹¹ and Tadeu Messias Donizete Borge¹²

ABSTRACT

The article investigates welding methods applied to Dual Phase (DP) steels, with emphasis on the DP1000 class, aimed at the automotive industry. DP steels, known for their high mechanical resistance due to their specific microstructure, are attractive for manufacturing lighter, stronger and safer vehicles. The welding method chosen was GMAW by conventional short circuit, due to its efficiency and low cost. The characterization used advanced optical microscopy techniques, scanning electron microscopy with EDS, EBSD, in addition to tensile and hardness tests. Microstructural analyzes using optical microscopy (OM), scanning electron microscopy (SEM) and EBSD confirmed the presence of ferrite, martensite and, occasionally, austenite in the base metal, as specified by the DP1000 steel manufacturer. The molten zone (ZF) showed variations in hardness, with values close to the thermally affected zone (TAZ) due to decarburization and the presence of alloying elements in the steel. Microstructural analysis of the weld beads by SEM identified proeutectoid ferrite, martensite and retained austenite. The changes in the microstructural and mechanical properties observed did not compromise the essential characteristics of the material, confirming that the short-circuit GMAW process proved to be suitable for applications in the automotive industry.

Keywords: GMAW, Microstructure, Conventional Short Circuit, DP1000, Welding.

¹ Education: Doctor in Mechanical Engineering

Educational Institution: Federal University of Uberlândia - UFU-MG

² Education: Doctor in Urban Engineering

Educational Institution: Federal University of São Carlos - UFSCar - SP

³ Education: Doctor in Science and Materials Engineering

Educational Institution: Federal Institute of Education, Science and Technology of Piauí - IFPI - PI

⁴ Education: Industrial Mechanical Engineering UFJF-MG

Educational Institution: Federal University of Juiz de Fora

⁵ Education: Mechanical Engineering

Educational Institution: Federal University of Juiz de Fora - UFJF-MG

⁶ Education: Post-Doctorate in Welding Engineering

Educational Institution: Federal University of Uberlândia - UFU-MG

⁷ Education: Doctor in Mechanical Engineering

Educational Institution: Federal University of Uberlândia - UFU-MG

⁸ Education: Doctor in Mechanical Engineering

Educational Institution: Federal University of Uberlândia - UFU-MG

⁹ Education: Doctor in Mechanical Engineering

Educational Institution: Federal University of Uberlândia - UFU-MG

¹⁰ Education: Master's Degree in Mechanical Engineering

Educational Institution: Federal University of Uberlândia - UFU-MG

¹¹ Education: Doctor in Mechanical Engineering

Educational Institution: Federal University of Uberlândia - UFU-MG

¹² Education: Doctor in Mechanical Engineering

Educational Institution: Federal University of Uberlândia - UFU-MG



INTRODUCTION

Climate change has intensified in recent decades, mainly due to human activities. This phenomenon, known as global warming, results in an increase in the average temperatures of the planet and oceans. The intensification of the greenhouse effect, caused by the higher concentration of gases such as carbon dioxide, methane, and nitrous oxide in the atmosphere, is the main cause of global warming (INTERGOVERNMENTAL PANEL ON CLIMATE CHANGE, 2018).

Emissions of these greenhouse gases reached new records in 2017, as reported by the U.S. National Oceanic and Atmospheric Administration (NOAA) and the American Meteorological Society (AMERICAN METEOROLOGICAL SOCIETY, 2018). In Brazil, vehicle emissions have increased significantly over the past two decades, with a growth of 192% between 1994 and 2014. According to a survey by the Institute of Energy and Environment in 2015, it is estimated that the car fleet in the country will double by 2030, reaching 88 megatons of carbon dioxide equivalent per year.

Faced with these challenges, the automotive industry has been looking for solutions to reduce the environmental impact of its products. The development of new metal alloys, such as Advanced High Strength Steel (AHSS), plays a crucial role in this mission. These steels, which combine high strength, good toughness, ductility, and formability, are ideal for the manufacture of lighter and safer vehicles (WORLD AUTO STEEL, 2017).

Fierce competition in the automotive industry means that material selection is driven by both cost and safety. Between 1980 and 2010, the percentage of steel used in vehicles increased from approximately 53% to 55% by weight, and today, about 60% of the materials in light vehicles in the North American industry are steel (TAMARELLI, 2017). This growth reflects the ability of AHSS steels to meet the performance and sustainability requirements of the industry.

Dual-Phase (DP) steels are especially valued in the automotive industry because they allow the reduction of vehicle mass, reducing the thickness of the plates and/or the specific densities, which contributes to the reduction of pollutant emissions at an affordable cost (SAMEK & KRIZAN, 2012). In addition, these steels offer excellent impact absorption, increasing passenger safety in the event of a collision (SHOME & TUMULUTU, 2015).

Despite the advantages, there are still challenges related to the weldability of DP steels, which need to be overcome for their wide application in the automotive industry. Non-standard welding parameters and the need to maintain strength and toughness in welded regions are critical issues (SHOME & TUMULUTU, 2015). The GMAW welding process, widely used for its high productivity, requires strict control of the parameters to ensure the quality of the welded joints (RODRIGUES, 2012).

Thus, this study aims to investigate the microstructural and mechanical changes of welded joints of Dual-Phase micro alloyed steel (DP1000), using the GMAW short-circuit welding process.



It seeks to ensure that the welded joints have good mechanical and metallurgical characteristics, adequate to the requirements of the automotive industry.

THEORETICAL FRAMEWORK

ADVANCED HIGH STRENGTH STEEL (AHSS)

Technological advances in processes such as continuous casting and thermomechanical processing have allowed the creation of advanced high strength steels (AHSS). These steels are characterized by their complex microstructures, which include hard islands of martensite, bainite and/or residual austenite dispersed in a ductile ferrite matrix. The combination and proportion of these phases are adjusted to produce the desired mechanical properties (Chatterjee & BHADSHIA, 2006).

AHSS steels are classified into different categories, each with specific characteristics that cater to diverse industrial applications. According to Keeler, Kimchi, and Mooney (2017), the main classes of AHSS include:

Dual Phase (DP) Steels: They combine ferrite and martensite, offering an excellent combination of ductility and strength.

Complex Phase (CP) steels: These contain a mixture of martensite, bainite and small amounts of residual austenite and ferrite.

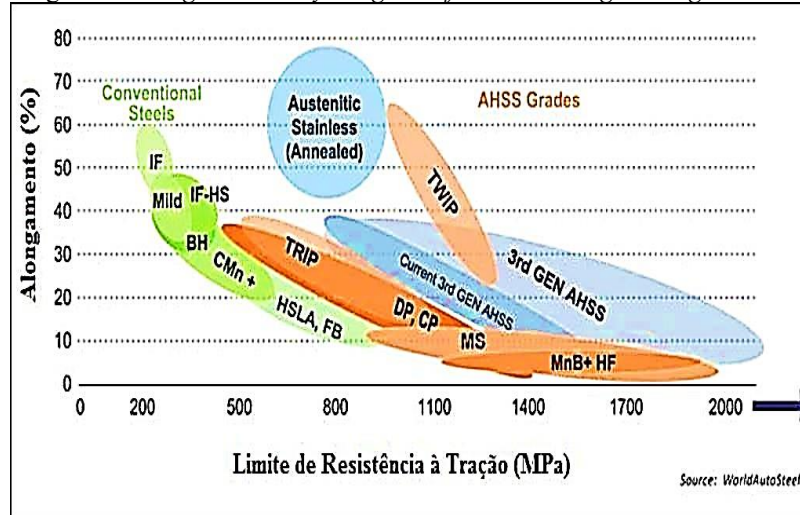
Transformation Induced Plasticity (TRIP) steels: These include ferrite, bainite and residual austenite that transforms to martensite under deformation, increasing ductility and strength.

Martensitic Steels (MS): Composed mainly of martensite, they provide high strength and are used in safety components that require high energy absorption.

AHSS has a higher tensile strength than HSLA (High-Strength Low-Alloy) steels, while maintaining the same ductility. Hardening mechanisms in AHSS include solid solution hardening, precipitation, grain refinement, and austenitic to martensitic phase transformation (BLECK, 2004). This makes AHSS ideal for automotive applications, especially in the production of shock-resistant structures where strength and energy absorption are essential (TASAN et al., 2015).

The multiphase microstructure of AHSS, composed of a ferrite matrix and islands of martensite, bainite, austenite and/or retained austenite, allows the fabrication of thinner sheets without compromising structural rigidity. Figure 1 shows the classification of strength levels as a function of elongation for the wide variety of grades of advanced high-strength steels.

Figure 1: Strength- Ductility Diagram of Advanced High Strength Steels.



Source: Adapted from Keeler and Kimchi (2017).

DUAL PHASE STEELS - DP

According to Kou (2020), Dual Phase (DP) steels are named based on their yield stress and tensile strength limit. For example, the DP500/800 grade indicates a steel with 500 MPa yield strength and 800 MPa tensile strength. Generally, these steels are classified by tensile strength limit and are commercially available in the range of 600 to 1200 Mpa.

The specific properties of DP steels are mainly attributed to their microstructure, which consists of martensite islands, a hard phase, embedded in a ferrite matrix, which is soft and ductile (CALCAGNOTTO *et al.*, 2011). The martensitic phase imparts strength, while the ferritic phase provides ductility. The volumetric fraction of martensite determines the strength level of the material, allowing these steels to achieve a tensile strength range between 500 and 1200 MPa (FONSTEIN, 2015).

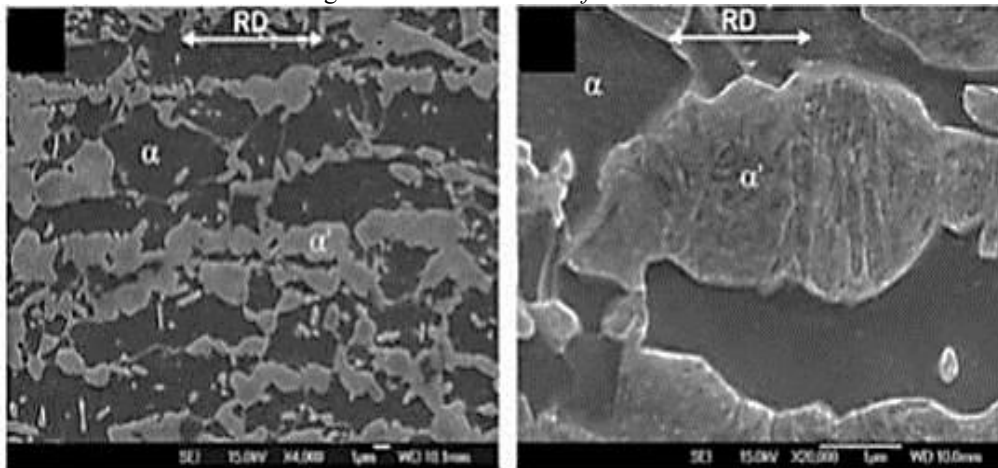
In addition to the traditional martensite and ferrite phases, other microstructural arrangements, such as bainite, austenite, and carbides, may be present, depending on the thermal processing route and chemical composition of the alloy (SEYEDREZAI *et al.*, 2014; GHASSEMI-ARMAKI *et al.*, 2014).

A wide range of mechanical properties can be adapted in DP steels by controlling factors such as martensite volumetric fraction, average carbon content and its distribution in martensite, ductility, martensite distribution, ferritic grain size, and alloying element content (ZHANG *et al.*, 2016).

Fonstein (2015) in his research comparing HSLA (High-Strength Low-Alloy) steels, DP steels contain more than 1% alloying elements. Its chemical composition varies, but the main alloying elements include carbon, manganese, and silicon. Other elements, such as aluminum, nitrogen, phosphorus, and sulfur, may also be present in smaller amounts. Dual Phase steel in general has additions of Mn and Si. Figure 2 shows the microstructure of a DP steel, where ferrite (α) is the darkest and lowest relief, while martensite (α') is the lightest phase and has the highest relief.

The martensitic regions promote hardening by dispersion following the law of mixtures, i.e., the higher the proportion of martensite, the more accentuated the generation of discordances in the ferrite around the martensite and the greater the mechanical strength of the material (KRAUSS, 2005). These discrepancies are generated by the shear and volume change associated with the transformation of austenite into martensite.

Figure 2: Microstructure of a DP steel.



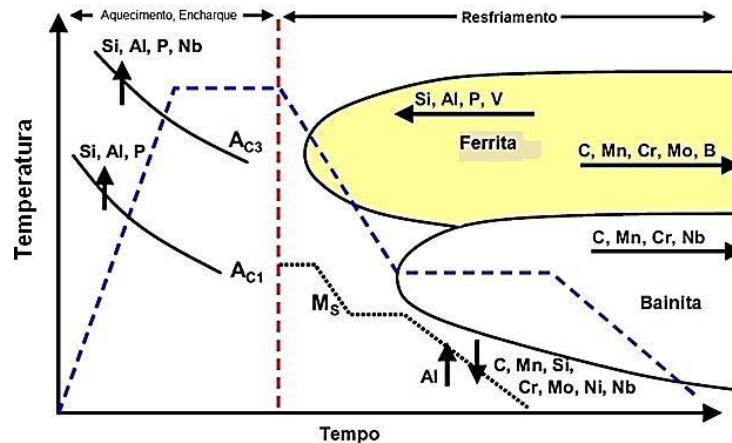
Source: Fonstein, et. al., 2015.

ALLOYING ELEMENTS OF DP'S STEELS

In DP's steels to acquire microstructures aiming at optimal mechanical properties, alloying elements are inserted, such elements control the volumetric fraction of martensite, which is formed after heat treatment of quenching and increase the strength of the steel by means of hardening mechanisms by solid solution and precipitation. Figure 3 shows the diagram of the effect of the insertion of alloying elements on the kinetics of phase transformations for advanced high-strength steels. It is verified that alloying elements can accelerate or slow down the transformation reactions and, in this way, influence the final microstructure of the material (ALLAM, 2015).

In terms of chemical composition, two-phase steels contain a carbon content in the range of 0.06-0.15% by weight (TASAN et al., 2015). This element has the function of hardening the martensite and stabilizing the austenite, delaying the transformation of ferrite and bainite, which allows slower cooling rates to obtain martensite, as can be interpreted by the analysis of figure 3. In addition, a low carbon content significantly improves the weldability and toughness of the material (SHI et al., 2014).

Figure 3: Schematic drawing of the effect of alloying elements on the temperature and kinetics of the phase transformation of AHSS



Source: Adapted from Allam (2015)

Typical manganese contents employed in two-phase steels range from 1.5 to 3% by weight. It is employed to delay the onset of austenite transformation and thus allow the use of slower cooling rates during quenching treatment. Manganese diffusion is substantially slower in austenite than in ferrite (Kuang et al., 2008). Therefore, if during intercritical annealing the soaking time is short, a concentration of manganese may occur in the austenite grain contours, which increases local hardening after heat treatment, as shown in figure 4.

Figure 4: Manganese-enriched region within a martensite particle



Source: Adapted from Kuang et al. (2008)

The use of microbinders such as vanadium, niobium and titanium aims to favor the precipitation hardening mechanism and promote the grain refinement of the microstructure. To increase hardenability, chromium and molybdenum can be added to the steel. These elements also decrease the transformation temperature of the bainite, thus limiting its formation.

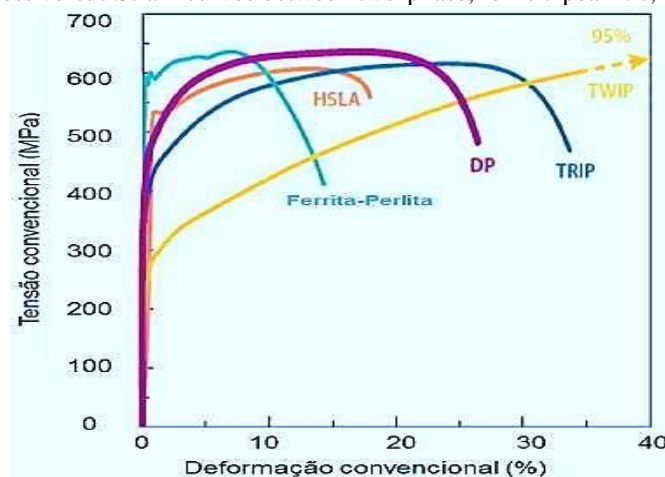
MECHANICAL PROPERTIES OF DP'S STEELS

Mechanical performance is the main factor driving the development of two-phase steels, as

these materials have good characteristics of mechanical strength, formability, continuous flow (absence of Lüders bands), high initial hardening rate and ductility (WANG *et al.*, 2013). It is these mechanical characteristics that allow two-phase steels to be increasingly used by the automotive industry to meet the demands of weight reduction and high crash resistance.

Tasan *et al.* (2015), established a comparison of the tensile properties between two-phase steels with ferritic-pearlitic, high-strength low-alloy (HSLA), TRIP and TWIP steels, as shown in Figure 5. In relation to the other steels analyzed, the two-phase steels demonstrated a unique behavior due to their microstructure being composed of a soft matrix of ferrite and martensite particles with high hardness. Although the newer advanced high-strength steel (AHSS) grades exhibit higher ductility, TRIP and TWIP steels, for now, have limited their use in the automotive industry due to factors such as: manganese segregation, high alloy cost and low weldability.

Figure 5: Comparison of Stress versus Strain curves between two-phase, ferritic-pearlitic, HSLA, TRIP and TWIP steels



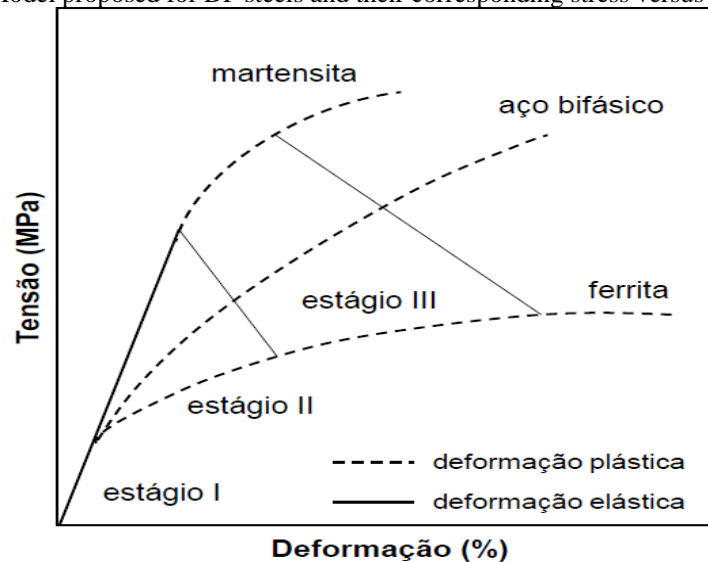
Source: Adapted from Tasan, et al. (2015)

DEFORMATION IN DP'S STEELS

Regarding deformation, Fonstein (2015) concluded that the behavior of two-phase steels is analogous to heterogeneous alloys that contain phases with substantially different mechanical properties and, therefore, can be considered composite materials. Thus, its mechanical properties are determined by the individual properties of the phases and their stereological parameters.

Figure 6 represents a deformation model diagram proposed for DP steels, which considers the individual behavior of the phases in relation to the deformation. According to Han *et al.*, (2011), the stress versus strain curve can be divided into three distinct stages. Stage I corresponds to the region in which ferrite and martensite deform elastically. In stage II, ferrite begins to undergo plastic deformation, while martensite continues to deform elastically. In stage III, the two phases deform plastically.

Figure 6: Model proposed for DP steels and their corresponding stress versus strain curves.



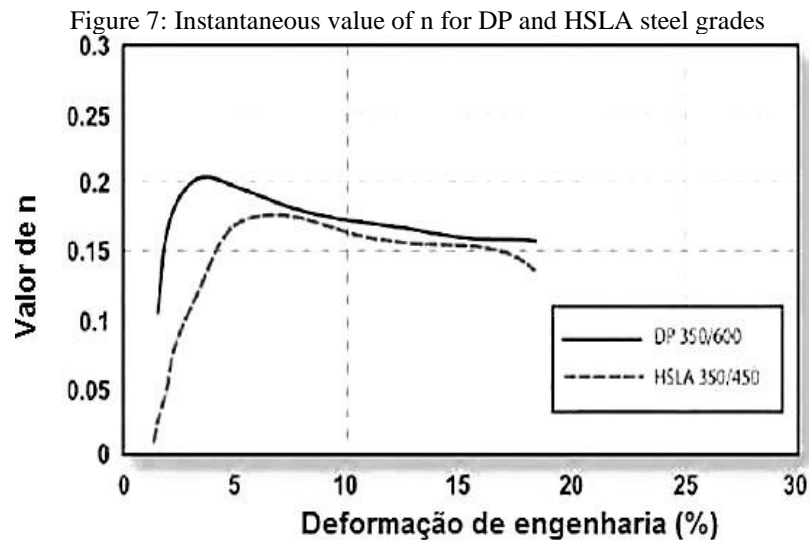
Source: Adapted from Han et al. (2011)

Initially, DP steels deform elastically up to the principle of continuous flow and high hardening rates, which determines the beginning of plastic deformation. As the plastic deformation continues, the hardening rate decreases until it reaches the resistance limit that determines the onset of plastic instability and, consequently, the rupture of the material.

HARDENING EXPONENT

The hardening exponent (n) is defined as the rate of increase in strength with plastic deformation. High n values are associated with good metal formability, since there is a more uniform distribution of deformations during the forming process, avoiding plastic instability and breakage. The main difference between two-phase (DP) steels and high-strength, low-alloy steels (HSLA) is that the former have high hardening exponent values and, therefore, are used in the manufacture of parts with more complex geometry for the automotive industry (DEMERI, 2013).

Conventional steels have a constant value for the hardening exponent as the deformations increase. Thus, n values were obtained in the strain range of 10 to 20%. Currently, some grades of advanced high-strength steels (AHSS) exhibit a hardening exponent that varies with deformation. Figure 7 shows the comparison of the n -value behavior between an HSLA 350/450 steel and a DP 350/600 steel. Two-phase steels are found to exhibit a high n value for small deformations. From deformations of the order of 7 to 8%, the values for the hardening exponent between two-phase steels and HSLA steels are approximated.



Source: Adapted from Demeri (2013)

The rapid hardening of two-phase steels can be attributed to three factors:

The residual stress generated during quenching heat treatment is relieved by plastic deformation;

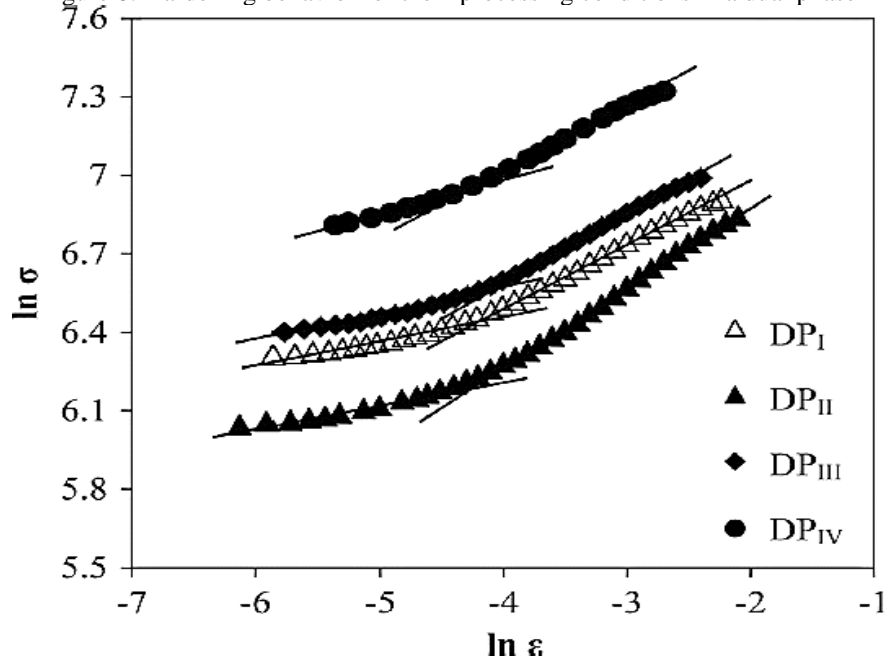
The increase in the density of disagreements in the ferritic matrix;

The plastic incompatibility between the ferrite and martensite phases causes compressive stresses in the ferrite, and these stresses restrict the displacement of the disagreements;

Figure 8 shows the hardening stages for a steel with a chemical composition of 0.17% C, 0.4% Si, 1.15% Mn and 0.95% Cr, with different thermomechanical processes analyzed by (MAZAHERI *et al.*, 2014).

In the DPI condition, the steel was initially heated to a temperature of 600°C for 20 minutes and cooled in water. It was then annealed at a temperature of 770°C for a period of 8 minutes and cooled in water. For the other three conditions, 600°C heating for 20 minutes was not applied. The intercritical annealing conditions used for these samples were: 770°C for a period of 8 minutes (DPII); 770°C for 10 minutes (DPIII) and 790°C for 8 minutes (DPIV). For all conditions, after annealing, cooling in water was carried out.

Figure 8: Hardening behavior for the 4 processing conditions in a dual phase



Source: Adapted from Mazaheri et al. (2014)

According to the author, the presence of different hardening stages in two-phase steels is related to the different activation mechanisms that occur for different strain intensities. In the first stage, with less inclination, the ferritic matrix deforms plastically while the martensite remains in the elastic regime. In the second stage, with greater inclination, the two phases deform plastically.

THE GMAW WELDING PROCESS

GMAW (Metal Arc Welding), also known as MIG/MAG (MIG – Metal Inert Gas) and (MAG – Metal Active Gas), is a welding process using an electric arc between the continuous feed wire-electrode and the weld pool. According to the American Welding Society – AWS (1991), the GMAW process uses an external gas shield without the application of pressure.

The welding process works with direct current (DC), in general it uses the wire on the positive pole (reverse polarity). In GMAW, welding currents from 50 A to 600 A, and welding voltages from 15 V to 32 V are commonly employed (SCOTTI & PONOMAREV, 2008).

According to Costa (2014), because it is a process that presents low current values during the open arc phase, and low voltage values, the heat transferred to the part is reduced, making the GMAW process suitable for applications that have as a requisite parts of small thickness, minimal distortion of the part, welding of tubular joints and stainless steels, that is, in operations that require low heat input.

With regard to direct polarity (wire on the negative pole) and alternating polarity, these are less used, as they require specific sources and techniques. Figure 9 shows an illustration of the GMAW soldering circuit:

Figure 9: GMAW Soldering Circuit



Source: Adapted from Lincoln Electric (2015a)

In the MIG/MAG welding process, different types of metals can be joined in different welding positions, in semi-automatic ways, or in mechanized/robotized/automated ways. API Standard 1104 (2010) conceptualizes mechanized welding as a process in which the parameters and orientation of the torch are controlled electronically or mechanically, but can be manually varied during welding to maintain the specified welding conditions.

With regard to semi-automatic welding, still according to API 1104 (2010), the equipment only controls the material feed and the welding progress is controlled manually. With automatic welding, the equipment is responsible for performing all operations without manual handling of the arc and welding speed, that is, without any interference from the operator, not depending on his manual skill.

Scotti & Ponomarev (2008) report that with respect to the use of an external gas shield, the appropriate flow for virtually all welding conditions is 10 to 16 l/min, and that values above these are usually inefficient. Regarding the thermal conductivity of the shielding gas, the temperature of the arc (plasma) influences its voltage, in the same way that it influences the thermal energy transferred to the pool, thus, the higher the thermal conductivity of the gas, the greater the welding voltage provided to sustain the arc, and with that, the greater the thermal energy. (FORTES, 2005).

In addition to pure shielding gases, mixtures are also commonly used. Additions of argon to carbon dioxide decrease the splash levels normally experienced with pure carbon dioxide. The mixture Argon + 21-25% CO₂ (C25) is universally known as the gas used in GMAW welding with short-circuit transfer. This mixture works well in high-current applications in thick materials, and can achieve good arc stability, weld pool control and bead appearance, as well as high productivity (FORTES, 2005).

METALLIC TRANSFER MODES

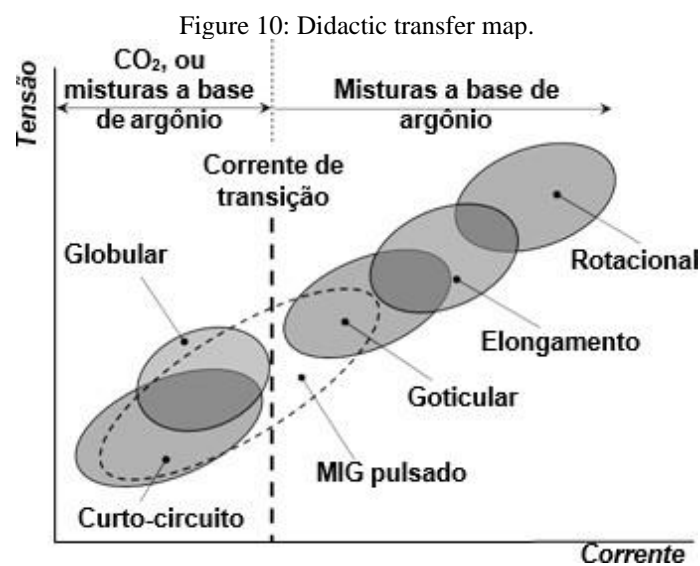
One of the main factors that influences the achievement of a good quality weld is the way the

material is transferred from the electrode (filler material) to the weld pool, that is, the mode of metal transfer (VILARINHO, 2007).

The modes of metallic transfer can be observed in the different welding processes, being associated with several factors, such as electrical parameters (voltage, type and polarity of the current), materials, gases, distance between the contact nozzle and the part (DBCP), specific characteristics of the power source, etc. (VILARINHO, 2007).

Scotti & Ponomarev (2008) subdivide the modes into two fundamental types of metal transfer in the GMAW process, the natural and the controlled mode. In natural transfer mode, metallic transfer varies "naturally" within a range of current and arc voltage levels. On the other hand, in the controlled transfer, the welding source is used to obtain current waveforms, so that the transfer "obeys" this controlled variation of the electrical parameters (VILARINHO, 2007).

The natural mode is classified into two transfer classes, short-circuit and free-flight (globular, goticular and explosive). In a more didactic way, it is possible to compile these transfer modes in a graph called a transfer map, as illustrated in Figure 10.



Source. Adapted from Vilarinho (2007)

In response to the technological advances in welding sources and control systems, the IIW (International Institute of Welding) has been proposing updates in the classification of metal transfer modes. Figure 10 represents the transfer modes according to the IIW classification for short-circuit transfer with increased current as one moves from modes A to E.

In short-circuit transfer, there is contact of the droplet with the puddle before its detachment. The main limitation of short-circuit transfer is the generation of spatter during the rupture of the liquid bridge between the electrode and the puddle by the Pinch Effect, which decreases the production capacity, either due to the loss of filler material or the need to spend resources for its removal (SOUZA, 2011). Good stability is obtained when using gases with CO₂ (lower cost and



higher thermal input) or Ar+CO₂ mixtures (lower splash level) (VILARINHO, 2007).

This short-circuit transfer mode is particularly useful for joining thin materials in any position, thick materials in the upright and overhead positions, and for filling wide openings. In short-circuit transfer welding, wires with diameters in the range of 0.8 mm to 1.2 mm are used, and small arc lengths (low voltages) and low welding currents are applied (FORTES, 2005).

In free flight transfer (globular, dropicular and explosive), the drop detaches before touching the pool, in which small drops of molten metal are detached from the end of the wire and projected by electromagnetic forces towards the weld pool (FORTES, 2005).

Globular transfer occurs when the molten metal droplets are too large and move towards the melt pool under the influence of gravity (FORTES, 2005). It is characterized by the use of low currents, but with a higher arc voltage and with a transfer frequency of less than 100 Hz (low and irregular). The weldments are limited to the flat position, with great arc instability, seriously limiting the use of this mode of transfer (VILARINHO, 2007).

Goticular transfer occurs when the current is increased above a level called transition current, seeking to maintain the same arc length. There will be a change in the mode of formation of the droplet in a small range of current (transition current), going from large drops at low frequency (globular) to small drops at high frequency (droplet), usually above 200 Hz (VILARINHO, 2007). It should be noted that the value of the transition current is a function of the material, diameter and length of the electrode, as well as the shielding gas and DBCP (VILARINHO, 2007).

METHODOLOGY

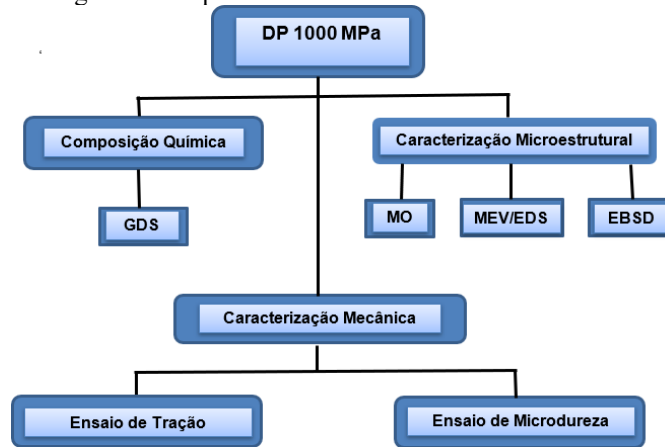
The purpose of this study was to investigate the microstructural and mechanical changes of Dual-Phase micro alloyed steel welded joints (DP1000), using the GMAW short-circuit welding process, ensuring that the welded joints presented microstructural and mechanical characteristics suitable for applications in the automotive industry. To achieve this goal, a methodology was adopted that included several stages.

Initially, experimental tests were carried out to characterize the base metal, aiming to understand its mechanical and microstructural properties. Then, the best parameters for the weld seams were selected, taking into account aspects such as welding speed and applied voltage. Based on these parameters, the final weld seams were made.

After the weld seams were made, they were subjected to qualification tests in order to verify their conformity with the required technical specifications. Finally, evaluations of the mechanical and metallurgical properties of the welded joints were carried out, using appropriate analytical techniques. Figure 11 shows the stages of characterization of the steel, used for the development of the research, such steps were carried out due to the need for more information on the base metal, as it

is a recently developed steel, and in figure 12, the stages of the experiments for analysis of the weld seams after welding are presented:

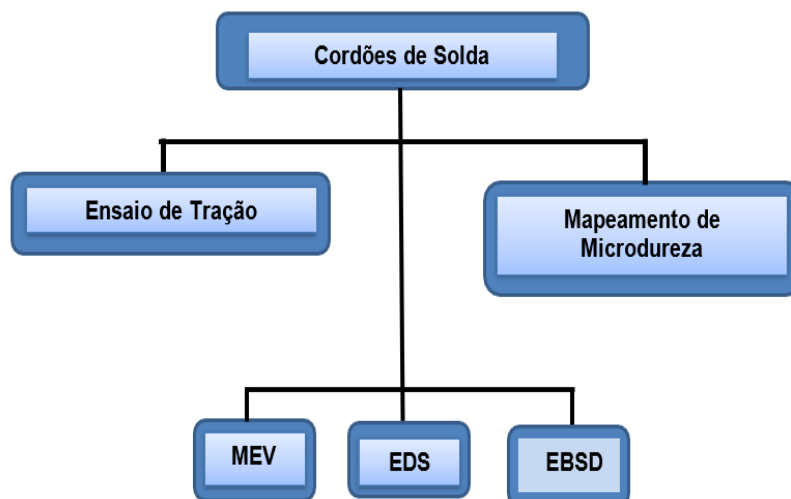
Figure 11: Steps for characterization of the base metal.



Source: Author (2024).

After the characterization stage of the base metal, a second stage was carried out aiming at the parameterization of the welding procedure, where carbon steel 16 was used as base metal, plate thickness of 1.50 mm, the welding speed parameter (V_s) was the preponderant factor for the choice of welding requirements, because it was sought a higher productivity in the process, Thus, as the result of macroscopic characterization to verify defects and possible points of improvement in parameterization.

Figure 12: Steps for characterization of Weld Beads.



Source: Author (2024).

RESULTS AND DISCUSSIONS

CHEMICAL COMPOSITION OF THE BASE METAL

The chemical composition of the Dual Phase 1000 Mpa resistance steel, performed by the Discharge and Gloss Spectrometer – GDS, is described in table 1, by percentage by weight of the chemical elements that compose them.

It was verified in the GDS analysis that the result obtained is in accordance with what is established for a Dual Phase microalloyed steel with resistance of the class of 1000 MPa, by the AHSS manufacturer's catalog.

Table 1. Chemical Composition of DP 1000MPa Steel (Percentage by Weight)

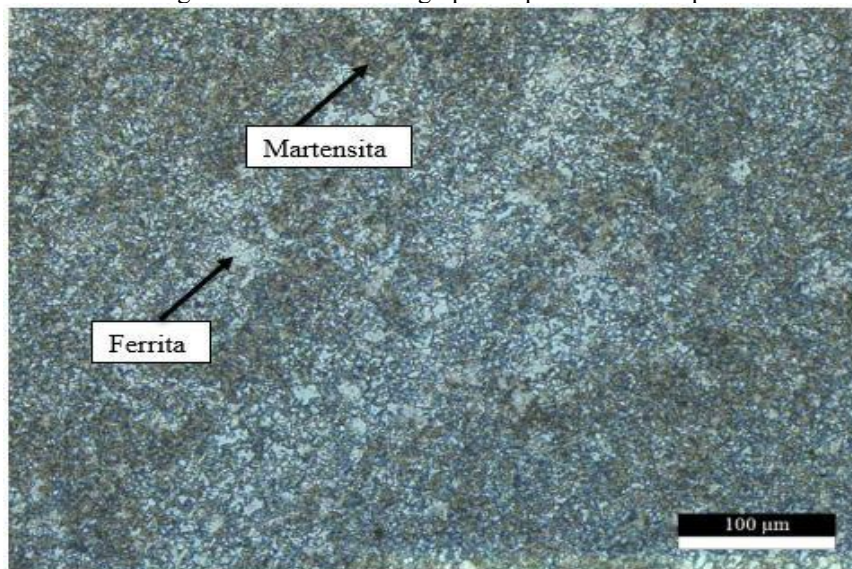
C	Oneself	Mn	P	S	Al	Cr	Mo	Nb	B
0,172	0,469	2,170	0,021	0,002	0,037	0,024	0,004	0,006	0,001

Source: Author (2024)

BASE METAL OPTICAL MICROSCOPY

In the optical microscopy analysis of DP 1000 steels, the presence of two predominant phases was verified, martensite (dark areas) and ferrite (light areas) phases, as shown in figure 7, these are in line with what is presented in the literature, which in general, defines DP steels as composed of a ferritic matrix with the presence of martensite islands (BLECK; PHIU-ON, 2009).

Figure 7: DP1000 Micrograph – Optical Microscope



Source: Author (2024)

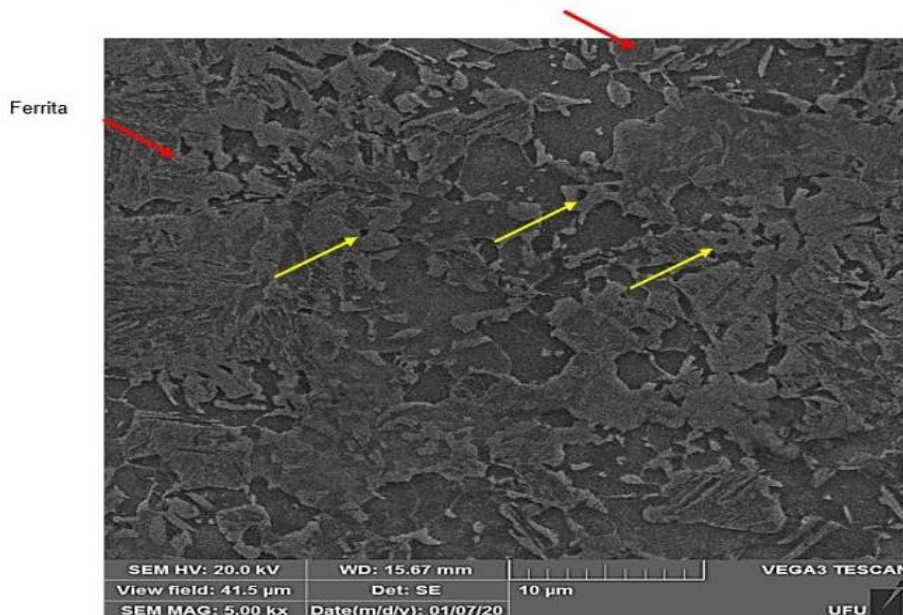
SCANNING ELECTRON MICROSCOPY AND ENERGY DISPERSIVE SPECTROSCOPY – SEM/EDS OF THE BASE METAL

In the SEM micrographs, a finer detail was observed in the distribution of martensite in the ferritic matrix, as shown in Figure 8. The distribution of martensite was not only limited to the

contours of the ferritic grains, but also to the grain contours, but also to the grain contours, and there were nucleation and growth sites of the previous austenite transformed into martensite on cooling. Particle-matrix interfaces are one of these preferred nucleation sites, as we can see for visible particles (FONSTEIN, 2015).

The distribution of martensite was not limited to the contours of the ferritic grains, as shown in figure 8, some ferritic grains showed martensite "islands" in their interior of different sizes and morphologies. It was verified that, in addition to the grain contours, there were nucleation and growth sites of previous austenite transformed into martensite on cooling. Particle-matrix interfaces are one of these preferred nucleation sites, as can be seen for visible particles (HUMPHREYS; HATHERLY, 2004). These visible particles can also be seen in Figure 8, represented by yellow arrows.

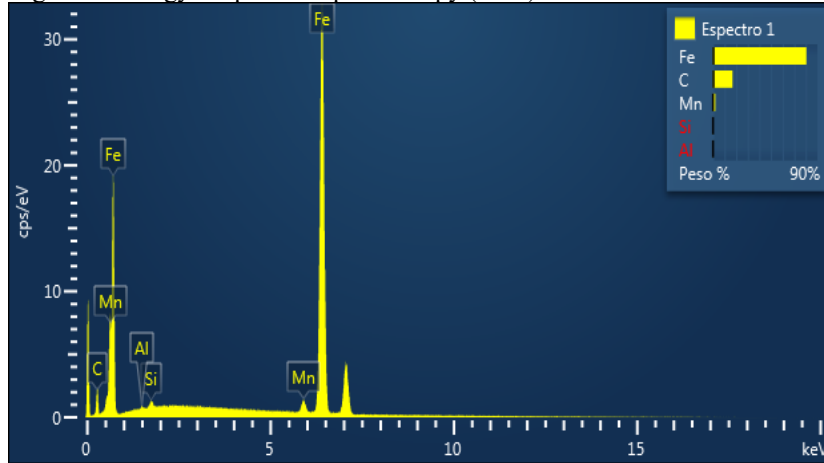
Figure 8: DP1000 micrograph, 5000x magnification – SEM
Martensita



Source: Author (2024)

The EDS analysis of the DP1000 samples showed that their results corroborated the GDS results, as shown in figure 9:

Figure 9: Energy Dispersive Spectroscopy (EDS) DP 1000 of the base metal.

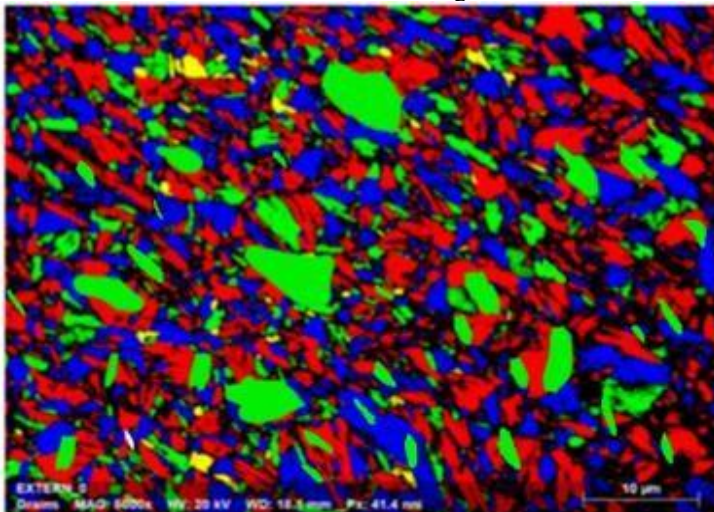


Source: Author (2024)

BACKSCATTERED ELECTRON DIFFRACTION – EBSD OF THE BASE METAL

The results of the EBSD analyses corroborate with the results of GDS, M.O, SEM and EDS, since they present, as shown in figure 10, the difference presented by the EBSD analyses is the detection of the presence of austenite microstructure, which was not possible to present in the M.O and SEM analyses, this can be justified by the equipment being more accurate in the detection of crystalline structures. Austenite is a solid solution of carbon in gamma iron, it is only stable at temperatures above 723 °C, unfolding by eutectoid reaction, at lower temperatures, in ferrite and cementite (CALLISTER & RETHWISCH. 2018).

Figure 10: EBSD DP1000



Phase Name	Raw	Norm
Austenite	5,32%	9,18%
Ferrite	58,37	83,9%
Martensite	6,81%	7,4%

Source: Author (2024)

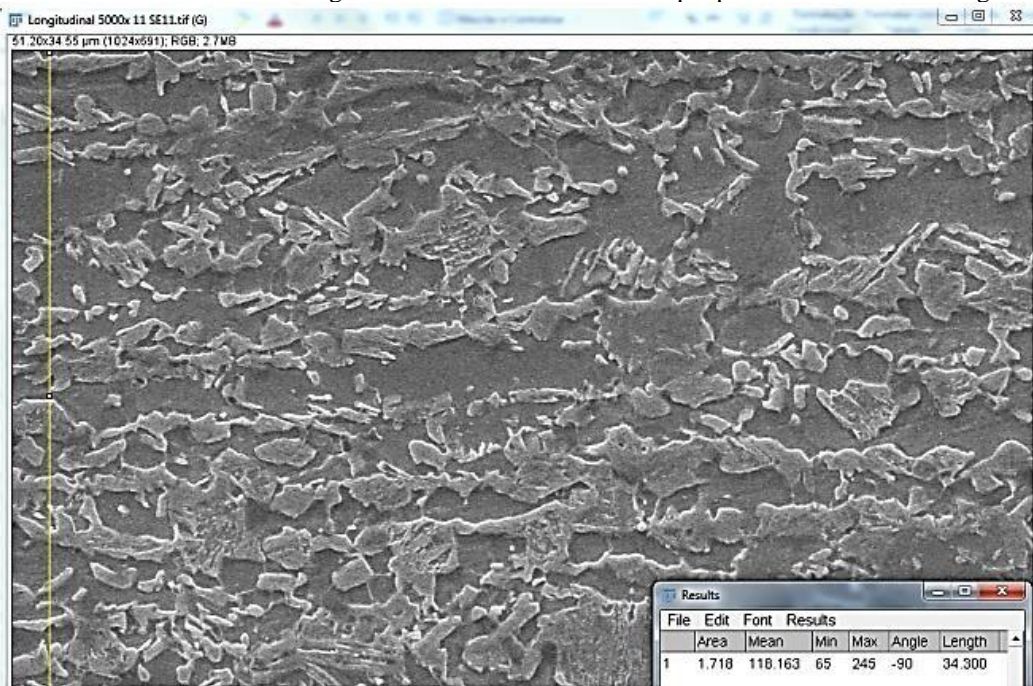
FERRITIC GRAIN SIZE ESTIMATION

The ferritic grain size estimate was performed according to the intercept method described in ASTM E112-13, as follows equation 1:

$$\text{Ferritic T.G.} = ((\text{test line length}) \times (\% \text{ ferrite})) / (\text{No. of grains}) \text{ (Eq. 1)}$$

Using the free program ImageJ, a test line was drawn in the horizontal direction and its length was defined. To determine the size of the ferritic grain, the number of ferritic grains intercepted by this line was counted. Figure 11 follows. The process was repeated twenty times with the displacement of the constant-size test line over twenty regions of the image. At the end of this step, the same procedure is carried out now by creating a test line in the vertical direction.

Figure 11: Determination of ferritic grain size in a DP1000 steel sample photo SEM at 5000x magnification.



Source: Author (2022)

Table 2 shows the estimates of ferritic grain sizes for the three directions studied: longitudinal, transverse and face.

Table 2. Ferritic grain size estimation

Direction	Average (μm)
Longitudinal	1,78
Transverse	1,36
Face	1,56

Source: Author (2024)

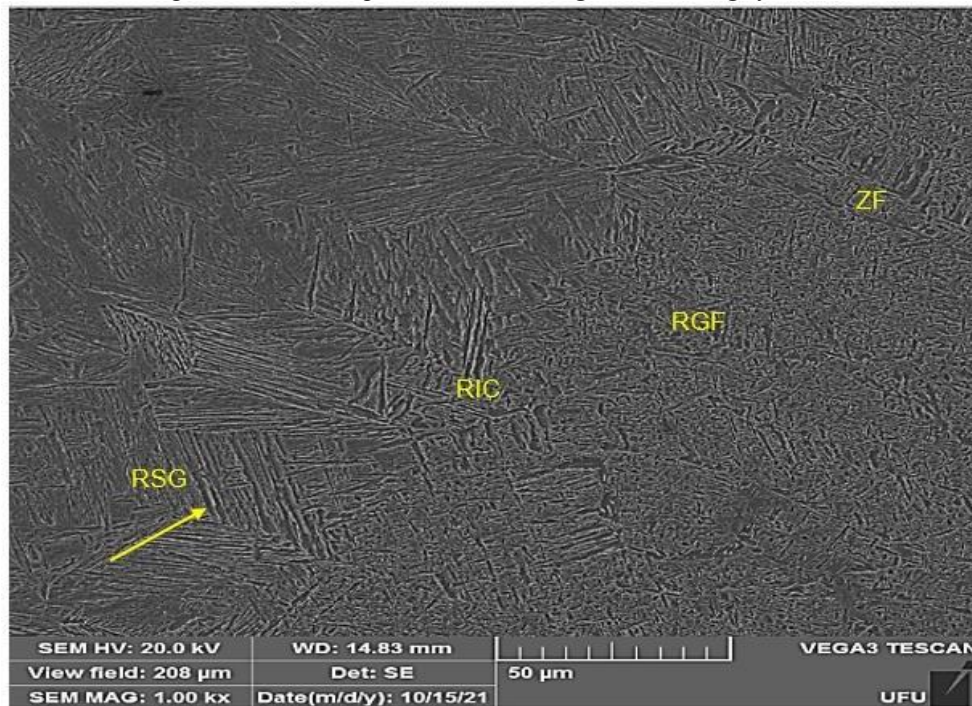
The ferritic grains are not equiaxial, so their average size is determined by the cube root of the product of the average size in each direction, according to equation 2, for the data in table 2, the average size of the ferrite grain was 1.56 μm .

$$\bar{l} = (\bar{l}_l \times \bar{l}_r \times \bar{l}_f)^{1/3} \text{ (Eq. 2)}$$

POST-WELDING SEM TESTS

The SEM analysis for the identification of microstructures was based on the Guide to the Light Microscope Examination of Ferritic Steel Weld Metals, prepared by IIW. Figure 12 shows the cross-section of the welded joint of DP1000 steel, an overview of the region mapped in the SEM, where it is possible to perceive the predominance of second-phase proeutectoid ferrite aligned in the ZF (molten zone), and in the initial position of the ZAC (RGF – fine-grained region). In the RIC zone, the presence of grain contour proeutectoid ferrite was observed, as well as the presence of martensite. In the RSG region, the predominance was of the proeutectoid ferrite microstructure with grain contour, and the presence of a smaller amount of acicular ferrite and martensite (yellow arrow) was also identified.

Figure 12: DP 1000 post-weld SEM image - 1000x magnification



Source: Author (2024)

CONCLUSION

Considering the objectives outlined in this study, the analysis of the GMAW process in DP1000 steel revealed the following conclusions:

Initial characterization of the materials revealed a ferritic matrix with martensite islands, as well as an average ferritic grain size of 1.56 µm and an average hardness of 313 HV. Microstructural analyses by M.O., SEM, and EBSD confirmed the presence of ferrite, martensite, and, in some cases,



austenite in the base metal. The results were consistent with the DP1000 steel manufacturer's requirements.

The experimental chemical composition was used to perform theoretical thermodynamic calculations of phase equilibrium and carbon equivalent. Thus, it was possible to determine the melting temperature for DP 1000 steel was 1512.31°C, the austenitization temperature (A1) was 928.81°C, and the carbon equivalent was 0.54, demonstrating that DP1000 steel has good weldability according to IIW.

The molten zone (ZF) showed variations in hardness, with some points close to the thermally affected zone (ZTA) showing similar values. This phenomenon can be attributed to the decarburization process and the presence of alloying elements in the steel. The SEM microstructural analysis of the weld seams revealed the presence of proeutectoid ferrite, martensite and retained austenite.

These conclusions highlight the feasibility of welding DP1000 steels using the GMAW process by conventional short circuit, highlighting that both the microstructural and mechanical properties have undergone modifications, however, these have not affected their primordial characteristics for use in the automotive industry.

ACKNOWLEDGMENT

I would like to thank CNPq for its support of the research; to the Federal University of Uberlândia – UFU for the opportunity for professional and intellectual growth; to Usiminas for having provided the material to be studied and made several experiments viable; to my advisor Prof. Dr. Louriel Oliveira Vilarinho for his support; and to my co-supervisor Prof. Dr. Ayrton de Sá Brandim for always believing in my potential.



REFERENCES

1. Allam, T. M. A. (2015). *Direct hot rolled dual phase weathering steel* (Tese de Doutorado, Universidade Técnica da Renânia do Norte - Vestfália, Aachen).
2. Angeli, J., Füredér, I., & Kneiss, G. (2006). Microstructural and mechanical properties of TRIP and DP steels. *Materials Science and Engineering: A, 441*(1-2), 1-17.
3. American Meteorological Society. (2018). *State of the Climate in 2017*.
4. American Petroleum Institute (API). (2010). *API 1104*.
5. Bleck, W. (2004). Using the TRIP effect – the dawn of a promising group of cold formable steels. *Steel Research International, 75*(10), 704-710.
6. Bleck, W., & Phiou-on, K. (2009). Effects of microalloying in multi phases steels for car body manufacture. In A. Haldar et al. (Eds.), *Microstructure and texture in steels and other materials* (pp. 145-163). Springer.
7. Callister, W., & Rethwisch, D. (2018). *Ciência e engenharia de materiais: uma introdução* (9ª ed.). LTC.
8. Calcagnotto, M., Ponge, D., Raabe, D., & Schreyer, A. (2011). Orientation gradients and geometrically necessary dislocations in dual-phase steel. *Acta Materialia, 59*(2), 658-670.
9. Chatterjee, S., & Bhadeshia, H. K. D. H. (2006). TRIP-assisted steels: cracking of retained austenite. *Materials Science and Technology, 22*(6), 641-644.
10. Costa, T. F. (2014). *Avaliação de Critérios de Estabilidade do Processo MIG/MAG Curto-circuito na Soldagem de Aços Inoxidáveis Austeníticos e Duplex* (Tese de Doutorado, Universidade Federal de Uberlândia).
11. Demeri, M. Y. (2013). *Advanced High-Strength Steels: Science, Technology, and Applications*.
12. Forte, C. (s.d.). *Apostila de Soldagem MIG/MAG – ESAB*.
13. Fonstein, N. (2015). *Advanced high strength sheet steels: physical metallurgy, design, processing, and properties*. Springer.
14. Ghassemi-Armaki, H., Zarei-Hanzaki, A., & Abedi, H. R. (2014). On the contribution of the microstructure to the work hardening behavior of a ferrite–martensite dual phase steel. *Materials Science and Engineering: A, 589*, 130-136.
15. Gorni, A. A., et al. (2008). Developments in AHSS for Automotive Applications. *Journal of Materials Engineering and Performance, 17*(3), 395-402.
16. Han, Q.-H., Kang, Y.-L., Zhao, X.-M., Lu, C., & Gao, L.-F. (2011). Microstructure and Properties of Mo Microalloyed Cold Rolled DP1000 Steels. *Journal of Iron and Steel Research International, 18*(5), 52-58.
17. Humphreys, F. J., & Hatherly, M. (2004). *Recrystallization and Related Annealing Phenomena* (2ª ed.). Pergamon.



18. Kou, S. (2020). **Welding Metallurgy**. Wiley.
19. Instituto de Energia e Meio Ambiente. (2015). **Emissões de Gases de Efeito Estufa no Brasil**.
20. Intergovernmental Panel on Climate Change. (2018). **Global Warming of 1.5°C**.
21. Keeler, S. P., Kimchi, M., & Mooney, P. (2017). **Advanced High-Strength Steels Application Guidelines**.
22. Kuang, S., Kang, Y. L., Yu, H., Liu, R. D. (2008). Simulation of intercritical austenization of a C-Mn cold rolled dual phase steel. **Materials Science Forum, 575**, 1062-1069.
23. Krauss, G. (2005). **Steels: Processing, Structure and Performance** (1st ed.). ASM International.
24. Kuziak, R., Kawalla, R., & Waengler, S. (2008). Advanced high strength steels for automotive industry. **Archives of Civil and Mechanical Engineering, 8*(2)*, 103-117.
25. Poggio, G. M., et al. (2005). Welding Parameters Optimization for Dual Phase Steels. **Welding Journal, 84*(4)*, 85-93.
26. Rodrigues, J. V. (2012). Welding Process Optimization in Automotive Industry. **Journal of Manufacturing Processes, 14*(2)*, 194-203.
27. Samek, J., & Krizan, D. (2012). Mechanical Properties of Advanced High Strength Steels (AHSS). **Materials and Manufacturing Processes, 27*(8)*, 835-840.
28. Seyedrezai, H., Pilkey, A. K., & Boyd, J. D. (2014). Effect of pre-IC annealing treatments on the final microstructure and work hardening behavior of a dual-phase steel. **Materials and Science Engineering A, 594**, 178-188.
29. Shaw, J. J., & Zuidema, J. (2001). Advanced High Strength Steels for Automotive Applications. **SAE Technical Paper Series, 2001-01-3035**.
30. Shome, M., & Tumulutu, V. (2015). Welding Challenges in High Strength Steel. **Journal of Materials Engineering and Performance, 24*(10)*, 3797-3804.
31. Shi, L., Yan, Z., Liu, Y., Zhang, C., Qiao, Z., Ning, B., & Li, H. (2014). Improved toughness and ductility in ferrite/acicular ferrite dual phase steel through intercritical heat treatment. **Materials Science & Engineering A, 590**, 7-15.
32. Souza, D., Rossi, M. L., Keocheguerians, F., Nascimento, V. C., Vilarinho, L. O., & Scotti, A. (Ano). Influência da Regulagem de Parâmetros de Soldagem sobre a Estabilidade do Processo MIG/MAG Operando em Curto-circuito.
33. Vilarinho, L. O. (2007). Modos Fundamentais de Transferência Metálica: Naturais e Controlados. **Revista da Soldagem**.
34. Tamarelli, C. M. (2017). **Advanced High-Strength Steels Application Guidelines**. WorldAutoSteel.
35. Tasan, C. C., Diehl, M., Yan, D., Bechtold, M., Roters, F., & Raabe, D. (2015). An overview of dual-phase steels: advances in microstructure-oriented processing and micromechanically guided design. **Annual Review of Materials Research, 45**, 391-431.



36. Wang, W., Li, M., He, C., Wei, X., Wang, D., & Dub, H. (2013). Experimental Study on High Strain rate Behavior of High Strength 600–1000 MPa Dual Phase Steels and 1200 MPa Fully Martensitic Steels. *Materials & Design, 47*, 510-521.
37. WorldAutoSteel. (2017). *Advanced High-Strength Steels Application Guidelines*.
38. Zhang, P., Liu, J., & Li, Y. (2016). Effect of martensite morphology on the mechanical properties of ferrite–martensite dual-phase steels. *Journal of Materials Engineering and Performance, 25*(6), 2548-2556.